

Hyper-VolTran: Fast and Generalizable One-Shot Image to 3D Object Structure via HyperNetworks

Christian Simon Sen He Juan-Manuel Pérez-Rúa Mengmeng Xu
Amine Benhalloum Tao Xiang
Meta

Abstract

Solving image-to-3D from a single view is an ill-posed problem, and current neural reconstruction methods addressing it through diffusion models still rely on scene-specific optimization, constraining their generalization capability. To overcome the limitations of existing approaches regarding generalization and consistency, we introduce a novel neural rendering technique. Our approach employs the signed distance function (SDF) as the surface representation and incorporates generalizable priors through geometry-encoding volumes and HyperNetworks. Specifically, our method builds neural encoding volumes from generated multi-view inputs. We adjust the weights of the SDF network conditioned on an input image at test-time to allow model adaptation to novel scenes in a feed-forward manner via HyperNetworks. To mitigate artifacts derived from the synthesized views, we propose the use of a volume transformer module to improve the aggregation of image features instead of processing each viewpoint separately. Through our proposed method, dubbed as **Hyper-VolTran**, we avoid the bottleneck of scene-specific optimization and maintain consistency across the images generated from multiple viewpoints. Our experiments show the advantages of our proposed approach with consistent results and rapid generation.

1. Introduction

Recent progress in neural 3D reconstruction has brought significant implications in various applications, *e.g.*, novel view synthesis [1, 32, 38, 39], and robotic vision [10, 13, 28, 37]. Specifically, there has been a growing interest in neural fields [1, 39, 44] to extract 3D information from multiple images given known camera parameters. NeRF [19] and the Signed Distance Function (SDF) [43] are image-to-3D reconstruction techniques [1, 2, 36] that produce plausible geometry and, hence, novel views. Despite great progress, achieving accurate 3D object reconstruction via neural implicit methods [1, 19, 43] still requires a substantial number of images featuring consistent view and appearance and pre-

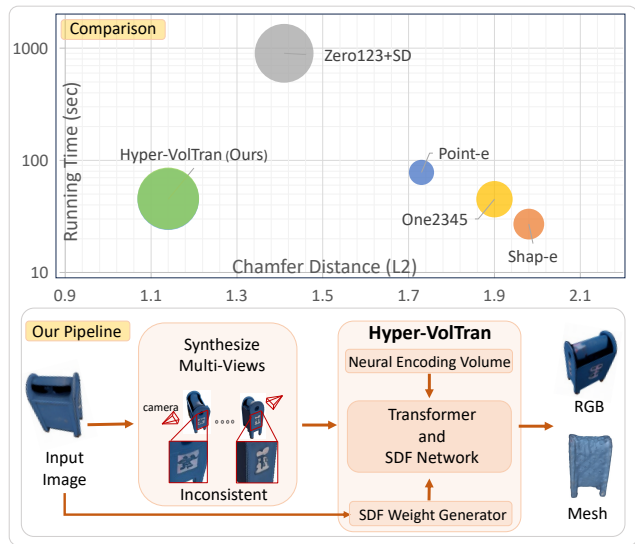


Figure 1. **Top:** Comparison of our proposed method against baselines on the running time and Chamfer Distance with the bubble area indicating IoU. **Bottom:** Our pipeline comprises two components for image-to-3D by synthesizing multi-views from a diffusion model and mapping from multi-views to SDFs using an SDF network with weights generated from a HyperNetwork.

cise camera poses to reconstruct 3D objects accurately.

In fact, collecting data from multiple views might not always be feasible when the resources are limited. Several works [2, 17, 44] demonstrate a capability to mitigate issues on 3D reconstruction under a sparse set of images. One key technique in these approaches is to build neural encoding volume projected from multiple input views. Though these techniques can perform on limited inputs, reconstructing 3D from a single image remains challenging and requires a strong prior to enabling the neural reconstruction model to produce plausible shapes and colors of unseen perspectives.

A recent development in generative models [4, 16, 26, 45] has shown promising results in 2D image generation that can act as a strong prior for unseen perspectives. Several

works approach this problem using the guidance of a diffusion model [21]. In particular, Poole *et al.* [21] introduce Score Distillation Sampling (SDS) [21] in which the neural reconstruction model learns through the feedback error from a diffusion model. The diffusion model is frozen without any updates while the NeRF [19] weights are updated during optimization. Even though this technique is capable of reconstructing 3D scenes, per-scene optimization is still required, which usually takes up to 1 hour to converge on a single GPU. This constraint restricts the practicality of this approach, particularly when it comes to efficiently performing 3D reconstruction. To achieve fast 3D reconstruction, a generalized prior that allows one feed-forward operation through the networks is required instead of relying on an expensive per-scene optimization.

An alternative method for rapid 3D reconstruction is to utilize a diffusion model and synthesize multi-view images. This can be achieved by leveraging a diffusion model that can produce images based on slight variations in camera parameters [16]. Nevertheless, creating images using a multi-view image generator (*e.g.*, Zero123 [16]) can be challenging in terms of preserving geometry consistency. Rather than optimizing a network for each object as in [21], we aim to preserve only one network to generalize for many objects. To achieve this, we can exploit neural encoding volume built from the projection of image features with known camera parameters as in [2, 17, 36]. While these approaches show promise, they still suffer from suboptimal results when employed for 3D reconstruction involving unseen objects.

In this work, we aim to address the aforementioned challenges, focusing on generalization, speed, and inconsistency issues. To this end, we introduce a neural network to address these concerns by employing an SDF network generated by HyperNetworks [9] and a Volume Transformer (VolTran) to alleviate the impact of inconsistent examples. Our approach explores the potential for generalization by introducing a latent variable obtained from an image encoder (*e.g.*, CLIP [23]) to yield image representations. Subsequently, we employ these image representations to generate the weights of the SDF, addressing the challenge of generalization. Please see Fig. 1 (bottom) for an illustration of our technique. To summarize, our contributions include:

1. We propose a generalizable prior for 3D mesh reconstruction with a few synthesized data by assigning the weights of SDFs based on the input image embedding.
2. We propose a transformer module for aggregation to enable working on inconsistent shapes and colors across different viewpoints.
3. We also show that our method only requires one feed-forward process and comfortably constructs a 3D mesh with negligible additional processing time ~ 5 seconds.

2. Related Work

Diffusion models for 2D to 3D reconstruction. Reconstructing a full 3D structure from only a few 2D images is challenging due to the inherent ill-posedness of the problem. However, recent advances in generative models and, in particular, diffusion models provide a promising direction toward obtaining the priors about the 3D world that are necessary to reconstruct the full 3D structure of an object from a single image. For example, they are used as an indirect way to provide feedback during the image-to-3D reconstruction process in [3, 18, 21, 33, 35]. A notable work so-called DreamFusion [21] proposes text-to-3D generation by Score Distillation Sampling (SDS), which allows optimization-guided generation of NeRF-parametrized [19] 3D scenes. A concurrent work using Score Jacobian Chaining [35] uses a similar approach, exploiting the chain rule on the outputs of a pretrained image generation model. Tang *et al.* [33] extend the idea with coarse and refining stages to enhance the outputs with textured point clouds. Recently, Zero123 [16] describes a diffusion model that takes an input image and camera parameters to synthesize a novel view. This model can generate more consistent multi-view images compared to an off-the-shelf diffusion model like Imagen [26]. Albeit a promising direction to reconstruct 3D models, per-scene optimization is still required and the neural implicit function is limited to represent only one object. Thus, the generalization of the trained model is limited for unseen objects.

Generalizable priors for fast 3D reconstruction. An ideal implementation of 3D reconstruction is a single model that can generalize to unseen objects, enabling 3D generation using a forward-pass approach only without applying further per-scene optimization. PixelNeRF [44] as a pioneer work in this direction proposes to extract feature volumes from an input image which are then passed through a NeRF model along with the camera extrinsic parameters. Chen *et al.* [2] present an approach called MVSNerf using cost volumes built of warped 2D image features and then regress volume density with a pass through an MLP (*i.e.*, neural encoding volumes) as the base geometry. Then, the neural encoding volume is used as an additional input to the NeRF model. SparseNeus [17] extends MVSNerf [2] to work on a few-data regime by proposing cascaded geometry reasoning to refine the details of a 3D object. However, this approach still requires multi-view inputs, with no obvious mechanism to extend it to a single image. To tackle the problem of 3D reconstruction from a single image, Liu *et al.* [15] propose a method called One2345 to exploit a diffusion model (*e.g.*, Zero123 [16]) to generate some example images with estimated camera poses. To improve the precision of the reconstructed geometric models, One2345 [15] employs SDFs [43] rather than NeRFs [19]. The challenge of this approach is inconsistency in generated examples,

making it difficult to reconstruct 3D scenes that fully respect the input appearance.

Another approach for avoiding per-scene optimization is to train a large-scale model with self-supervised learning and make use of large-scale labeled text-to-3D data. Point-e [20], a system to generate 3D point clouds from text description, is a pioneer in this direction. Following up this work, Shap-e [11] directly generates the weights of the neural implicit model that can be rendered as meshes and radiance fields. This method generates multiple synthetic images then a neural 3D reconstruction technique (*e.g.*, SDF [43] or NeRF [19]) is employed to produce 3D models. This model cuts the cost of image-to-3D reconstruction from several GPU hours to 1-2 minutes. While this method can produce results quickly, the quality of the reconstructed 3D surfaces remains subpar. Unlike all these prior works, our proposed method can generate accurate 3D reconstruction with competitive processing time (*i.e.*, less than 1 minute).

Context-based learning. In few-shot learning, the concept of leveraging contextual information for achieving optimal performance across diverse input conditions is a well-established idea, as indicated by previous works like [7, 9, 29–31, 40]. Some of these methods involve model parameter updates through gradient descents, exemplified by several works [7, 46]. However, these approaches still require multiple feed-forward operations to update the model. Our focus lies in developing an approach that accomplishes context understanding with just a single feed-forward operation, without the need for additional optimization steps. To achieve this, we opt to adopt context-based information by generating neural network weights. Specifically, we draw inspiration from HyperNetworks [9] designated to generate neural network weights based on the provided context.

3. Proposed Method

Our 3D neural reconstruction pipeline has two streams, as shown in Fig. 2. Given a single-view image and its depth map, we first synthesize multi-view images via a diffusion model. Then, as shown in the upper stream of the figure, the synthesized images are fed into a neural encoding volume to obtain the 3D geometry representation of its structure. The geometry representation is combined with the images to predict a rendered RGB map by our proposed transformer module, VolTran. Meanwhile, we also use the synthesized multi-view images in a HyperNetwork to estimate an SDF weight, shown in the bottom stream. The SDF network predicts SDFs for surface representations that will later be used for rendering the depth map and extracting the mesh. Therefore, we name our approach **Hyper-VolTran**.

3.1. One to multiple-view images

We begin our pipeline by leveraging a pretrained generative model. This enables us to expand a single input image into

multiple views from a broader set of object viewpoints, albeit with some imperfections. For fair comparison, we strictly follow the approach outlined in [16] to leverage elevation and azimuth conditioning.

Synthesized views. Given a single RGB image and its corresponding depth map denoted as $I \in \mathbb{R}^{H \times W \times 3}$, and $D \in \mathbb{R}^{H \times W}$, respectively, we follow Zero123 [16] to normalize its shape and use a spherical camera system for the depth map. We apply an off-the-shelf image generation model to create N RGB images and depth maps sampled uniformly from several viewpoints according to ground-truth camera parameters [15]. Concretely for training, we form a set of RGB images and depth maps of an object as the source set $\mathcal{I} = \{I_1, \dots, I_N\}$ and $\mathcal{D} = \{D_1, \dots, D_N\}$. Note that both RGB and depth images are used as training targets to supervise the model in the training stage. However, those depth maps are omitted in the testing phase.

3.2. Geometry-Aware Encoding

Geometry-aware encoding is essential in building a generalized method for surface prediction from multi-view images. Our approach employs neural encoding volumes [2, 41] to construct 3D geometry based on the diversified input views from Sec. 3.1 and their associated camera poses. To this end, we warp 2D image features from the N input images onto a localized plane situated within the reference view’s frustum.

Neural encoding volume. In deep multi-view stereo [41, 42], 3D geometry can be inferred in the form of Cost Volume construction. Let $f_\theta : \mathbb{R}^{H \times W \times 3} \rightarrow \mathbb{R}^{H \times W \times C}$ be the mapping from an input image to a feature map. Similar to [17, 41], we encode images using a Feature Pyramid Network [14] as the mapping function to extract a neural feature map, *i.e.*, $F_i = f_\theta(I_i)$. Besides, we partition the scene’s bounding volume into a grid of voxels. Then, along with the intrinsic and extrinsic camera parameters $P = [K, R, t]$ for each image I_i , the neural feature map is projected based on each vertex v , and the output is denoted as $F_i(\Pi_i(v))$, where $\Pi_i(v)$ projects $v \in \mathbb{R}^3$ onto the local plane by applying P [41]. In particular, the homography warping is applied for each view i , and the final neural encoding volume G can be computed as Eq. 1.

$$G = \phi \left(\text{Var} \left(\{F_i(\Pi_i(v))\}_{i=1}^N \right) \right). \quad (1)$$

Here $\text{Var}(\{F_i(\Pi_i(v))\}_{i=0}^{N-1})$ is the Cost Volume, Var means the variance over N viewpoints, and ϕ denotes a function responsible for regularizing and propagating scene information instantiated as a sparse 3D CNN (*i.e.*, Geometry Guided Encoding). Since the variance accommodates differences in the image appearance among multiple input perspectives, G acquires the ability to encode complex 3D scene geometry

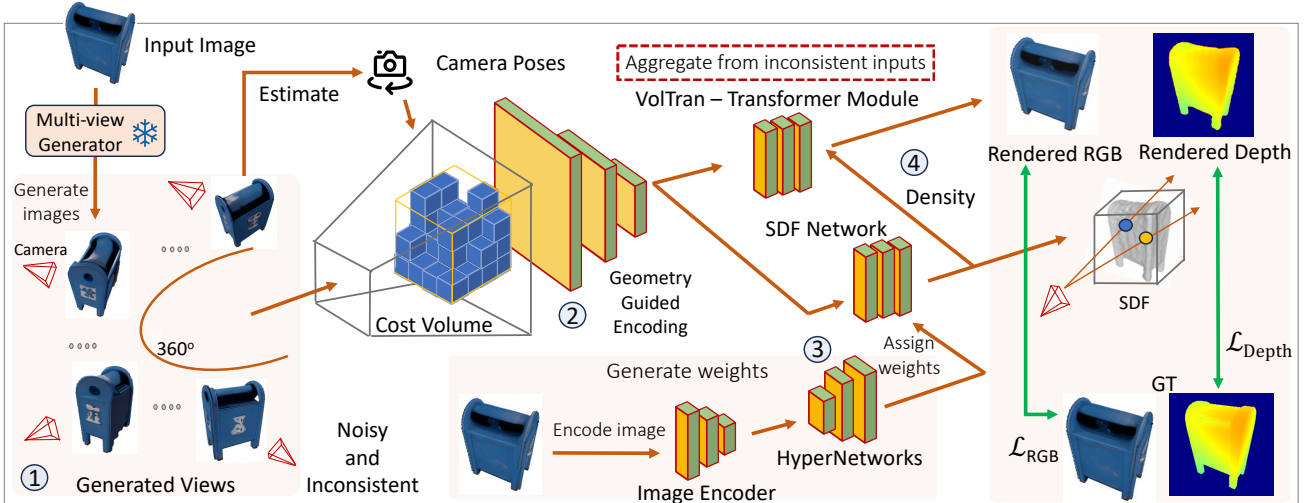


Figure 2. **Our training pipeline starts from a single image. Expanding a single view to an image set using a viewpoint-aware generation model, our method employs supervised learning with RGB and depth regression losses.** Specifically, 1) Utilizing N RGB images and depth maps, we generate additional viewpoints and camera poses. 2) Geometry-Guided Encoding is derived from warped image features in the form of a Cost Volume. 3) Instead of test-time optimization, we obtain SDF weights with a single pass of a HyperNetwork module, considering image appearance through visual encoding. 4) The geometry-encoded volume and the image features are passed to the SDF network and a transformer module to reveal the complete 3D object structure. Hence, our method Hyper-VolTran encompasses quick adaption to novel inputs thanks to our HyperNetwork design and consistent structures from global attention.

and appearance from diversified images. Thus, these volume features contain appearance-aware information that can be later used for volume rendering and SDF predictions.

3.3. Volume Rendering

A neural encoding volume previously computed is employed to predict both the density and view-dependent radiance at arbitrary locations within a scene. Next, this facilitates the utilization of differentiable volume rendering to predict the colors of images. For volume rendering, we opt to use SDF [43] instead of NeRF [19] for a more accurate surface reconstruction.

Signed Distance Function (SDF). SDFs represent 3D surfaces using a positional function that provides the nearest distance to the surface. Given an arbitrary 3D location in our setup, we use an MLP $f_{\Psi} : \mathbb{R}^d \rightarrow \mathbb{R}$ as an SDF to represent 3D surfaces. Although the generic SDF input has $d = 3$ as the signed distance is associated with a point $z \in \mathbb{R}^3$, our method uses a higher d as the input consists of the concatenation of feature from neural encoding volumes, colors, and image features. Another limitation of the generic SDF is the lack of generalization ability. For example, when using the neural encoding volume as an input, we can train an SDF network on a large collection of 3D objects [2, 17] to avoid per-scene optimization. In testing, however, the SDF network is usually frozen [15, 17] and limited to the known

objects. We propose a more adaptable approach to dynamically assign MLP’s weights based on the generated outputs of a HyperNetworks [9], which is conditioned on the input image.

HyperNetworks for an SDF network. HyperNetworks [9] constitute a neural model that generates the weights for a target network designed to generalize on various tasks given a context. Rather than preserving a neural network fixed during test time, HyperNetwork offers a mechanism to assign weights based on a condition dynamically. Mathematically, we design a HyperNetwork module $\delta_l(\cdot)$ to produce the weight for each layer ψ_l of the SDF network f_{Ψ} :

$$\psi_l = \delta_l(\xi(I_1)). \quad (2)$$

To encode the input image, we use a pretrained image encoder ξ that reduces the image dimensionality from RGB space to a latent space. Unlike the past work [6] that needs to optimize neural networks for every single object, our method trains the module on the fly without requiring per-scene optimization and directly calculating losses between two neural network parameters. Since our condition is the feature representation of the input object, our HyperNetwork can produce a more dedicated and appropriate weight for its target network. On the other hand, as we utilize the output of the Hypernetwork [9] to assign weights to the SDF network, our model generalizes better on the new object during inferences,

especially when the object shares similar semantics with the training data. Moreover, the hypernetworks are directly updated with a loss from RGB and depth map in our pipeline. Thus, we do not have to store the individual optimal weight parameter after per-scene optimization.

Rendering from SDFs. To estimate the parameters of the neural SDF and color field, we adopt a volume rendering method from NeuS [36] to render colors and volumes based on the SDF representations. For a given pixel, we describe M emitted rays from that pixel as $\{\mathbf{p}(t) = \mathbf{o} + t\mathbf{v} | t \geq 0\}$, with \mathbf{o} being the camera’s focal point and r representing the ray’s unit direction. We feed the combined features through an MLP and employ the *softmax* function to derive the blending weights denoted as $\{\omega_i\}_{i=1}^N$. The radiance at a given point \mathbf{p} and viewing direction \mathbf{v} is calculated as the weighted sum in Eq 3.

$$\hat{\mathbf{c}} = \sum_{i=1}^N \omega_i \cdot \mathbf{c}_i, \quad (3)$$

where \mathbf{c}_i is the color of source view i . Given the radiance, our volume rendering strategies is expressed in Eq 4.

$$\hat{\mathbf{C}} = \sum_{j=1}^M T_j \alpha_j \hat{\mathbf{c}}_j, \quad (4)$$

$$\alpha_j = 1 - \exp\left[-\int_{t_j}^{t_{j+1}} \rho(t) dt\right]. \quad (5)$$

Here, $T_j = \prod_{k=1}^{j-1} (1 - \alpha_k)$ is a discrete accumulated transmittance, α_k is the discrete opacity, and $\rho(t)$ denotes opaque density. The rendered depth map can be derived as Eq. 6:

$$\hat{\mathbf{D}} = \sum_{j=1}^M T_j \alpha_j t_j. \quad (6)$$

Note the rendering process is fully differentiable; we train the pipeline in a supervised manner so that the model can predict the rendered colors $\hat{\mathbf{C}}$ and depths $\hat{\mathbf{D}}$ in inference.

VolTran: multi-view aggregation transformer. Pixel data is inherently confined to a local context and lacks broader contextual information, frequently leading to inconsistent surface patches, particularly in the case of sparse input data. One trivial solution is to aggregate features across different views to capture the projected features from multiple views. Unfortunately, the synthesized views might be corrupted due to the flaws in the generative model, a simple aggregation [15, 17, 41] (e.g., average and max. pooling) might fail to render shapes and colors accurately. We propose a transformer module called *VolTran* based on the self-attention design in [34] to encode global information

from different N viewpoints. Besides the inputs, we learn an aggregation token as an extra token to obtain a corresponding output for a target view. Formally, let $\mathbf{X} \in \mathbb{R}^{N+1 \times d}$ be a matrix with rows composed of the tokens from source views and the aggregation token by concatenating the feature from color \mathbf{c}_i , image feature $\mathbf{F}_i(\Pi(\mathbf{v}))$, and volume feature \mathbf{G} yielding the dimension d . We denote $f_V(\cdot), f_Q(\cdot), f_K(\cdot)$ as functions to map values, queries, and keys of a transformer module. Thus, the aggregation operation can be calculated by the self-attention module, as shown in Eq. 7:

$$\text{Attn}(\mathbf{X}) = \text{Softmax}(\mathbf{A}) f_V(\mathbf{X}), \quad (7)$$

where $\mathbf{A}_{i,j} = f_Q(X_i)^\top f_K(X_j) / \gamma$ for all $i, j \in [N]$. As we apply multi-head attention, it can be formulated as $\text{MHA}(\mathbf{X}) = [\text{Attn}_1(\mathbf{X}), \dots, \text{Attn}_3(\mathbf{X})] \mathbf{W}_H$. We opt to use LayerNorm to normalize the intermediate activations and skip connection to stabilize training. The final output from the transformer module, an MLP, is introduced as a mapping function to obtain the blending weight ω_i . Afterwards, the final color can be obtained as in the SDF rendering pipeline.

3.4. Training and Inference

Our framework has several losses to train the model, including the HyperNetwork module. Every module is optimized in an end-to-end fashion only in the training stage. We define our loss for rendered colors with mean squared error *w.r.t.* the ground-truth \mathbf{C}_i :

$$\mathcal{L}_{\text{RGB}} = \frac{1}{|P|} \sum_{i=1}^{|P|} \|\hat{\mathbf{C}}_i - \mathbf{C}_i\|_2^2. \quad (8)$$

In addition to the color loss, we also calculate depth predictions supervised with the following loss:

$$\mathcal{L}_{\text{Depth}} = \frac{1}{|P_1|} \sum_{i=1}^{|P_1|} |\hat{\mathbf{D}}_i - \mathbf{D}_i|. \quad (9)$$

Also, in order to regularize the SDF values derived from the SDF network f_Ψ , we compute the Eikonal loss [8]:

$$\mathcal{L}_{\text{Eikonal}} = \frac{1}{|\mathbb{V}|} \sum_{\mathbf{v} \in \mathbb{V}} (\|\nabla f_\Psi(\mathbf{v})\|_2 - 1)^2, \quad (10)$$

where \mathbf{v} is a sampled 3D point and $\nabla f_\theta(\mathbf{v})$ is the gradient relative to the sample point q . This loss impacts the surface smoothness.

Furthermore, to empower our framework for generating concise geometric surfaces, we incorporate a sparsity regularization term that penalizes uncontrollable surfaces called a sparse loss [17], expressed as follows:

$$\mathcal{L}_{\text{Sparse}} = \frac{1}{|\mathbb{V}|} \sum_{\mathbf{v} \in \mathbb{V}} \exp(-\tau |s(\mathbf{v})|), \quad (11)$$

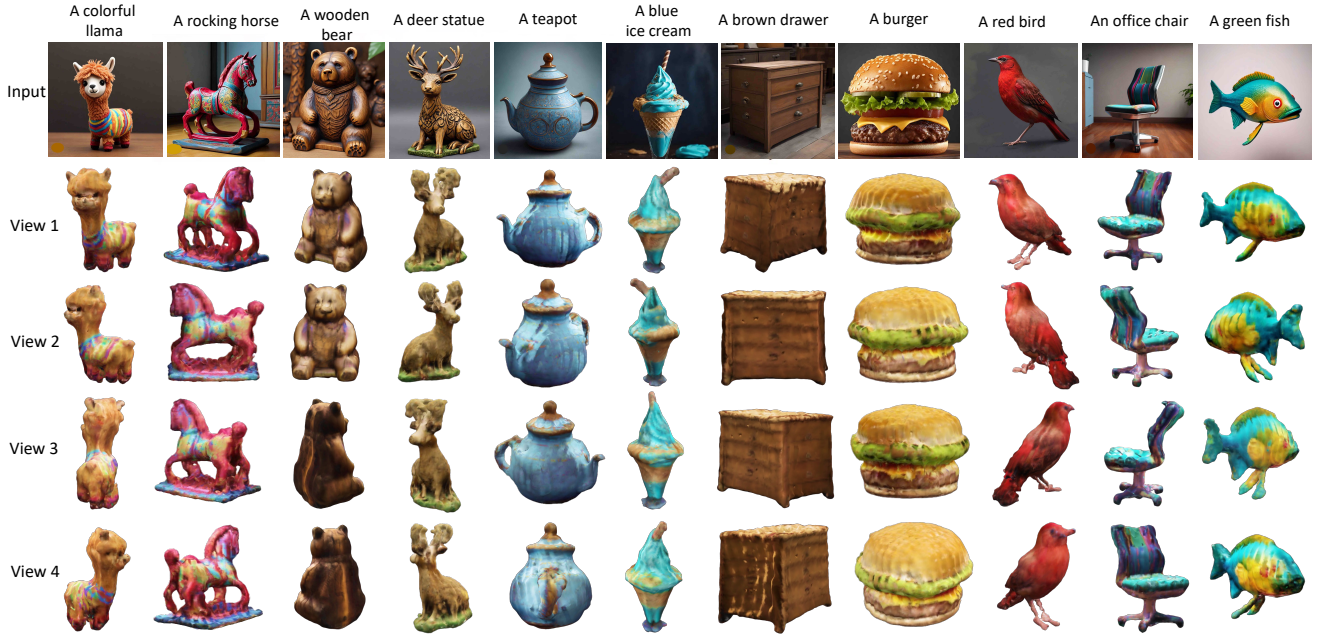


Figure 3. **Qualitative results of Hyper-Voltran on text-to-3D colored meshes.** The generated images from a diffusion model are used as inputs. We only focus on the main object of the input image.

where $s(v)$ is the predicted SDF and τ is the hyperparameter to scale the SDF prediction. To summarize, The total loss is defined as $\mathcal{L}_{RGB} + \mathcal{L}_{Depth} + \beta_1 \mathcal{L}_{Eikonal} + \beta_2 \mathcal{L}_{Sparse}$.

Inference. During inference, there is no more optimization, and only one feed-forward is performed, which reduces the expensive computation to update the models during testing. First, given an input image, we segment the input to extract the foreground object. After we obtain the object with clear background (e.g., white color), we synthesize multi-view scenes from the pretrained Zero123 model [16] conditioned on the relative change of camera viewpoints. These synthesized images are then employed to generate a 3D mesh by our proposed method. The inference of our proposed method only contains feed-forward, thus comfortably reducing the computational time compared to the existing distillation methods [18, 21, 27].

4. Experiments

4.1. Implementation details

We train our models from publicly available data first shared by [15], containing 46K synthesized 3D scenes. For the base multi-view generative model, we follow Zero123 [16] and keep its weights frozen. Additionally, for the geometry-guided encoder, we set the volume encoding size to $96 \times 96 \times 96$ for all of our experiments. For the SDF weight generation, we employ the CLIP model [23] as the image encoder, known for generating dependable representations.

In terms of the loss function, we verified that the setting proposed by [17] is optimal, i.e., $\beta_1 = 0.1$ and $\beta_2 = 0.02$. On the other hand, during inference, we first apply image segmentation to get an accurate cutout of the target object using the Segment Anything Model (SAM) [12]. Then, we generate 8 key views which are further extended by 4 nearby images each, for a total of 32 viewpoints.

4.2. Text-to-3D Results

The text-to-3D pipeline is performed by using off-the-shelf text-to-image models e.g., [24, 26, 45]. We apply the corresponding diffusion process conditioned on a given prompt (e.g., "a wooden bear") and obtain an image depicting it. To handle unexpected background information, we cut out the target object from the generated image using SAM [12]. Different views are further synthesized alongside corresponding camera poses using Zero123 [16]. The full set of generated images are fed to our model, constructing neural encoding volume, generating SDF network weights through a HyperNetwork, and applying global attention, the main components of Hyper-VolTran. Fig. 3 shows results of our method across different views for a given text prompt. It can be observed from these images that Hyper-Voltran produces good quality meshes that adhere well to corresponding texture, giving a sense of consistency across views.

4.3. Image-to-3D Results

We use a subset of the GSO dataset [5] to quantitatively evaluate one-shot image-to-3D mesh, comprising 25 objects



Figure 4. **Qualitative comparison on single image to 3D reconstruction with previous works** *e.g.*, One2345 [15], Shap-e [11], Point-e [20], and Zero123+SD [21]. VolTran offers more consistent and higher-quality results than competitors, generally providing a higher level of preservation of input details. Please see our supplementary material for more results and zoomed-in details.

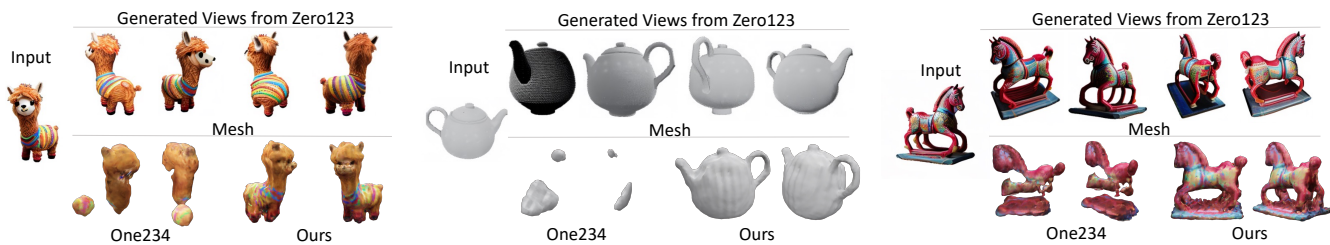


Figure 5. Examples of inconsistently generated views and comparison of our proposed method against One2345 [15] in generating meshes. One2345 fails to build well-reconstructed meshes when the views are arguably inconsistent and challenging.

from different GSO categories. For evaluating rendering quality, we use images from [18], spanning 15 objects.

Qualitative results. We offer qualitative demonstrations of our approach and comparison to One2345 [15], Shap-e [11], Point-e [20], and Zero123+SD [16] in Fig. 4, showcasing Hyper-Voltran’s efficacy in addressing one-shot image-to-3D object reconstruction. For a fair comparison with One2345 [15], we employ the same set of synthesized images to generate the 3D meshes. We note that One2345 [15] showcases inaccurate and unnatural shapes in Fig. 4. Also, we compare to other feed-forward-only approaches [11, 20]. Point-e and Shap-e cannot successfully reconstruct 3D meshes from a single image yielding incorrect colors and

shapes. Our proposed method is proven robust across a varied set of different objects with higher fidelity and more accurate shapes compared to the baselines. We also show in Fig. 5 some inconsistencies in generated images from Zero123 [16] and how our method can robustly construct the meshes compared to the baseline.

Quantitative results. To evaluate our method and compare against baselines in generating meshes, we use the PyTorch3D [25] package to calculate Chamfer distance and Iterated Closest Point for source and target alignment to compute F-score. In terms of metrics, we follow prior works [15], and [5], and use F-Score, Chamfer L2 distance, and intersection-over-union (IoU). These metrics are sum-

Method	F-Score (\uparrow)	Chamfer L2 (\downarrow)	IoU (\uparrow)	Time
Point-e [20]	16.45	1.73	0.09	78 secs
Shap-e [11]	10.10	1.98	0.11	27 secs
Zero123+SD [16]	14.85	1.41	0.21	15 mins
One2345 [15]	12.00	1.90	0.13	45 secs
Hyper-VolTran (ours)	17.45	1.14	0.22	45 secs

Table 1. F-Score, Chamfer L2, IoU, and time comparison to baselines on the GSO dataset [5].

Method	PSNR (\uparrow)	LPIPS (\downarrow)	CLIP Sim. (\uparrow)
Point-e [20]	0.98	0.78	0.53
Shap-e [11]	1.23	0.74	0.59
Zero123 [16]	19.49	0.11	0.75
RealFusion [18]	0.67	0.14	0.67
Magic123 [22]	19.50	0.10	0.82
One2345 [15]	16.10	0.32	0.57
Hyper-VolTran (ours)	23.51	0.10	0.86

Table 2. PSNR, LPIPS, and CLIP similarity comparison to prior works on the collected images in RealFusion [5].

marized in Table 1, where Hyper-VolTran proves its improved generalization capabilities on unseen objects by scoring higher than competitors across all tracks, at reasonable computation time cost. Similarly, for rendering quality, our method tops all previous works on 3D rendering across all scores: PSNR, LPIPS, and the CLIP similarity score as shown in Table 2.

Processing Time. Although our proposed method relies on encoding the input image through an image embedding model and generating weights of the SDF network, the full 3D generation latency is only around 5 seconds on a single A100 GPU. This is on par with the processing time of One2345 [15]. Additional latency is due to the base diffusion model. In our case, we opt to use Zero123 [16] for the synthesis of additional views, adding on average around 40 seconds per object. As shown in Table 1, the processing time of Shap-e is lower, which results in generally lower quality results than our method.

4.4. Analysis and Ablations

The SDF weight generator via a HyperNetwork and VolTran. We investigate the efficacy of our proposed two modules: the HyperNetwork for SDF and VolTran. This ablation study is performed to analyze the impact of each module. As shown in Fig. 6, we can observe that rendering deteriorates without the HyperNetwork and VolTran. While without VolTran, rendering scenes yields some noise as the impact of inconsistent inputs. Using both, we can achieve plausible rendering results.



Figure 6. Ablation study on each module. Impacts of each module on rendering colored scenes.

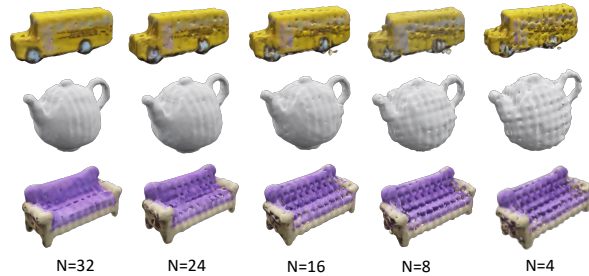


Figure 7. Qualitative results with different numbers of samples generated from a diffusion model. The more images are generated from the diffusion model, the better shape quality is achieved.

Number of samples. We evaluate the generated results by varying numbers of support images obtained from the diffusion model, ranging from 32 down to 4 images from different perspectives. Fig. 7 showcases the impact of the number of samples generated from the diffusion model. Our approach gains advantages from an increased number of generated images for forming geometry representations. Conversely, an excessively low number of samples leads to degradation.

5. Conclusions

In this paper, we address the challenge of deriving a 3D object structure from a single image. Our proposed approach, called Hyper-VolTran, comprises a HyperNetwork module and a transformer module. Specifically, HyperNetworks generate SDF weights, while the transformer module facilitates robust global aggregation from inconsistent multi-views. Our method demonstrates effective generalization to unseen objects in the single image-to-3D task, as evidenced by both quantitative and qualitative evaluations. Notably, our approach rapidly generates 3D meshes, accomplishing this task in just 45 seconds without per-scene optimization. Compared with state-of-the-art methods, our proposed approach excels in both time efficiency and reconstruction accuracy.

References

- [1] Jonathan T. Barron, Ben Mildenhall, Matthew Tancik, Peter Hedman, Ricardo Martin-Brualla, and Pratul P. Srinivasan. Mip-nerf: A multiscale representation for anti-aliasing neural radiance fields, 2021. **1**
- [2] Anpei Chen, Zexiang Xu, Fuqiang Zhao, Xiaoshuai Zhang, Fanbo Xiang, Jingyi Yu, and Hao Su. Mvsnerf: Fast generalizable radiance field reconstruction from multi-view stereo. *arXiv preprint arXiv:2103.15595*, 2021. **1, 2, 3, 4**
- [3] Rui Chen, Yongwei Chen, Ningxin Jiao, and Kui Jia. Fantasia3d: Disentangling geometry and appearance for high-quality text-to-3d content creation. In *Proceedings of the IEEE/CVF International Conference on Computer Vision (ICCV)*, 2023. **2**
- [4] Yuren Cong, Mengmeng Xu, Christian Simon, Shoufa Chen, Jiawei Ren, Yanping Xie, Juan-Manuel Perez-Rua, Bodo Rosenhahn, Tao Xiang, and Sen He. Flatten: optical flow-guided attention for consistent text-to-video editing. *arXiv preprint arXiv:2310.05922*, 2023. **1**
- [5] Laura Downs, Anthony Francis, Nate Koenig, Brandon Kinman, Ryan Hickman, Krista Reymann, Thomas B. McHugh, and Vincent Vanhoucke. Google scanned objects: A high-quality dataset of 3d scanned household items, 2022. **6, 7, 8**
- [6] Ziya Erkoç, Fangchang Ma, Qi Shan, Matthias Nießner, and Angela Dai. Hyperdiffusion: Generating implicit neural fields with weight-space diffusion. *arXiv preprint arXiv:2303.17015*, 2023. **4**
- [7] Chelsea Finn, Pieter Abbeel, and Sergey Levine. Model-agnostic meta-learning for fast adaptation of deep networks. In *Proceedings of the 34th International Conference on Machine Learning*, pages 1126–1135, 2017. **3**
- [8] Amos Gropp, Lior Yariv, Niv Haim, Matan Atzmon, and Yaron Lipman. Implicit geometric regularization for learning shapes. In *Proceedings of Machine Learning and Systems 2020*, pages 3569–3579, 2020. **5**
- [9] David Ha, Andrew M. Dai, and Quoc V. Le. Hypernetworks. *CoRR*, abs/1609.09106, 2016. **2, 3, 4**
- [10] Benran Hu, Junkai Huang, Yichen Liu, Yu-Wing Tai, and Chi-Keung Tang. Nerf-rpn: A general framework for object detection in nerfs. In *IEEE/CVF Conference on Computer Vision and Pattern Recognition (CVPR)*, 2023. **1**
- [11] Heewoo Jun and Alex Nichol. Shap-e: Generating conditional 3d implicit functions, 2023. **3, 7, 8**
- [12] Alexander Kirillov, Eric Mintun, Nikhila Ravi, Hanzi Mao, Chloe Rolland, Laura Gustafson, Tete Xiao, Spencer Whitehead, Alexander C. Berg, Wan-Yen Lo, Piotr Dollár, and Ross Girshick. Segment anything. *arXiv:2304.02643*, 2023. **6**
- [13] Stanley Lewis, Jana Pavlasek, and Odest Chadwicke Jenkins. NARF22: Neural articulated radiance fields for configuration-aware rendering. In *International Conference on Intelligent Robots and Systems (IROS)*. IEEE, 2022. **1**
- [14] Tsung-Yi Lin, Piotr Dollár, Ross B. Girshick, Kaiming He, Bharath Hariharan, and Serge J. Belongie. Feature pyramid networks for object detection. In *CVPR*, 2017. **3**
- [15] Minghua Liu, Chao Xu, Haiyan Jin, Linghao Chen, Mukund Varma T, Zexiang Xu, and Hao Su. One-2-3-45: Any single image to 3d mesh in 45 seconds without per-shape optimization, 2023. **2, 3, 4, 5, 6, 7, 8**
- [16] Ruoshi Liu, Rundi Wu, Basile Van Hoorick, Pavel Tokmakov, Sergey Zakharov, and Carl Vondrick. Zero-1-to-3: Zero-shot one image to 3d object. In *Proceedings of the IEEE/CVF International Conference on Computer Vision (ICCV)*, pages 9298–9309, 2023. **1, 2, 3, 6, 7, 8**
- [17] Xiaoxiao Long, Cheng Lin, Peng Wang, Taku Komura, and Wenping Wang. Sparseneus: Fast generalizable neural surface reconstruction from sparse views. *ECCV*, 2022. **1, 2, 3, 4, 5, 6**
- [18] Luke Melas-Kyriazi, Christian Rupprecht, Iro Laina, and Andrea Vedaldi. Realfusion: 360 reconstruction of any object from a single image. In *Arxiv*, 2023. **2, 6, 7, 8**
- [19] B Mildenhall, PP Srinivasan, M Tancik, JT Barron, R Ramamoorthi, and R Ng. Nerf: Representing scenes as neural radiance fields for view synthesis. In *European conference on computer vision*, 2020. **1, 2, 3, 4**
- [20] Alex Nichol, Heewoo Jun, Prafulla Dhariwal, Pamela Mishkin, and Mark Chen. Point-e: A system for generating 3d point clouds from complex prompts. *arXiv preprint arXiv:2212.08751*, 2022. **3, 7, 8**
- [21] Ben Poole, Ajay Jain, Jonathan T. Barron, and Ben Mildenhall. Dreamfusion: Text-to-3d using 2d diffusion. *arXiv*, 2022. **2, 6, 7**
- [22] Guocheng Qian, Jinjie Mai, Abdullah Hamdi, Jian Ren, Aliaksandr Siarohin, Bing Li, Hsin-Ying Lee, Ivan Skokhodov, Peter Wonka, Sergey Tulyakov, and Bernard Ghanem. Magic123: One image to high-quality 3d object generation using both 2d and 3d diffusion priors. *arXiv preprint arXiv:2306.17843*, 2023. **8**
- [23] Alec Radford, Jong Wook Kim, Chris Hallacy, Aditya Ramesh, Gabriel Goh, Sandhini Agarwal, Girish Sastry, Amanda Askell, Pamela Mishkin, Jack Clark, Gretchen Krueger, and Ilya Sutskever. Learning transferable visual models from natural language supervision. *CoRR*, abs/2103.00020, 2021. **2, 6**
- [24] Aditya Ramesh, Prafulla Dhariwal, Alex Nichol, Casey Chu, and Mark Chen. Hierarchical text-conditional image generation with clip latents, 2022. **6**
- [25] Nikhila Ravi, Jeremy Reizenstein, David Novotny, Taylor Gordon, Wan-Yen Lo, Justin Johnson, and Georgia Gkioxari. Accelerating 3d deep learning with pytorch3d. *arXiv:2007.08501*, 2020. **7**
- [26] Chitwan Saharia, William Chan, Saurabh Saxena, Lala Li, Jay Whang, Emily Denton, Seyed Kamyar Seyed Ghasemipour, Raphael Gontijo-Lopes, Burcu Karagol Ayan, Tim Salimans, Jonathan Ho, David J. Fleet, and Mohammad Norouzi. Photorealistic text-to-image diffusion models with deep language understanding. In *Advances in Neural Information Processing Systems*, 2022. **1, 2, 6**
- [27] Junyoung Seo, Wooseok Jang, Min-Seop Kwak, Jaehoon Ko, Hyeonsu Kim, Junho Kim, Jin-Hwa Kim, Jiyoung Lee, and Seungryong Kim. Let 2d diffusion model know 3d-consistency for robust text-to-3d generation. *arXiv preprint arXiv:2303.07937*, 2023. **6**
- [28] Anthony Simeonov, Yilun Du, Lin Yen-Chen, , Alberto Rodriguez, , Leslie P. Kaelbling, Tomas L. Perez, and Pulkit

- Agrawal. Se(3)-equivariant relational rearrangement with neural descriptor fields. In *Conference on Robot Learning (CoRL)*. PMLR, 2022. 1
- [29] Christian Simon, Piotr Koniusz, Richard Nock, and Mehrtash Harandi. On modulating the gradient for meta-learning. In *ECCV*, 2020. 3
- [30] Christian Simon, Piotr Koniusz, Richard Nock, and Mehrtash Harandi. Adaptive subspaces for few-shot learning. In *Proceedings of the IEEE/CVF Conference on Computer Vision and Pattern Recognition (CVPR)*, 2020.
- [31] Christian Simon, Piotr Koniusz, and Mehrtash Harandi. Meta-learning for multi-label few-shot classification. In *Proceedings of the IEEE/CVF Winter Conference on Applications of Computer Vision (WACV)*, pages 3951–3960, 2022. 3
- [32] Mukund Varma T, Peihao Wang, Xuxi Chen, Tianlong Chen, Subhashini Venugopalan, and Zhangyang Wang. Is attention all that neRF needs? In *The Eleventh International Conference on Learning Representations*, 2023. 1
- [33] Junshu Tang, Tengfei Wang, Bo Zhang, Ting Zhang, Ran Yi, Lizhuang Ma, and Dong Chen. Make-it-3d: High-fidelity 3d creation from a single image with diffusion prior, 2023. 2
- [34] Ashish Vaswani, Noam Shazeer, Niki Parmar, Jakob Uszkoreit, Llion Jones, Aidan N. Gomez, Lukasz Kaiser, and Illia Polosukhin. Attention is all you need. *CoRR*, abs/1706.03762, 2017. 5
- [35] Haochen Wang, Xiaodan Du, Jiahao Li, Raymond A. Yeh, and Greg Shakhnarovich. Score jacobian chaining: Lifting pre-trained 2d diffusion models for 3d generation. *arXiv preprint arXiv:2212.00774*, 2022. 2
- [36] Peng Wang, Lingjie Liu, Yuan Liu, Christian Theobalt, Taku Komura, and Wenping Wang. Neus: Learning neural implicit surfaces by volume rendering for multi-view reconstruction. *NeurIPS*, 2021. 1, 2, 5
- [37] Bowen Wen, Jonathan Tremblay, Valts Blukis, Stephen Tyree, Thomas Muller, Alex Evans, Dieter Fox, Jan Kautz, and Stan Birchfield. Bundlesdf: Neural 6-dof tracking and 3d reconstruction of unknown objects. *CVPR*, 2023. 1
- [38] Francis Williams, Zan Gojcic, Sameh Khamis, Denis Zorin, Joan Bruna, Sanja Fidler, and Or Litany. Neural fields as learnable kernels for 3d reconstruction. *CoRR*, abs/2111.13674, 2021. 1
- [39] Ziyang Xie, Junge Zhang, Wenye Li, Feihu Zhang, and Li Zhang. S-neRF: Neural radiance fields for street views. In *The Eleventh International Conference on Learning Representations*, 2023. 1
- [40] Mengmeng Xu, Yanghao Li, Cheng-Yang Fu, Bernard Ghanem, Tao Xiang, and Juan-Manuel Perez-Rua. Where is my wallet? modeling object proposal sets for egocentric visual query localization. *arXiv preprint arXiv:2211.10528*, 2022. 3
- [41] Yao Yao, Zixin Luo, Shiwei Li, Tian Fang, and Long Quan. Mvsnet: Depth inference for unstructured multi-view stereo. *European Conference on Computer Vision (ECCV)*, 2018. 3, 5
- [42] Yao Yao, Zixin Luo, Shiwei Li, Jingyang Zhang, Yufan Ren, Lei Zhou, Tian Fang, and Long Quan. Blendedmvs: A large-scale dataset for generalized multi-view stereo networks. *Computer Vision and Pattern Recognition (CVPR)*, 2020. 3
- [43] Lior Yariv, Jiatao Gu, Yoni Kasten, and Yaron Lipman. Volume rendering of neural implicit surfaces. In *Advances in Neural Information Processing Systems*, pages 4805–4815. Curran Associates, Inc., 2021. 1, 2, 3, 4
- [44] Alex Yu, Vickie Ye, Matthew Tancik, and Angjoo Kanazawa. pixelnerf: Neural radiance fields from one or few images. In *CVPR*, 2021. 1, 2
- [45] Lili Yu, Bowen Shi, Ramakanth Pasunuru, Benjamin Muller, Olga Golovneva, Tianlu Wang, Arun Babu, Binh Tang, Brian Karrer, Shelly Sheynin, Candace Ross, Adam Polyak, Russell Howes, Vasu Sharma, Puxin Xu, Hovhannes Tamoyan, Oron Ashual, Uriel Singer, Shang-Wen Li, Susan Zhang, Richard James, Gargi Ghosh, Yaniv Taigman, Maryam Fazel-Zarandi, Asli Celikyilmaz, Luke Zettlemoyer, and Armen Aghajanyan. Scaling autoregressive multi-modal models: Pretraining and instruction tuning. *arXiv:2309.02591*, 2023. 1, 6
- [46] Luisa M Zintgraf, Kyriacos Shiarlis, Vitaly Kurin, Katja Hofmann, and Shimon Whiteson. Fast context adaptation via meta-learning. 2019. 3

**** Supplementary Material ****
Hyper-VolTran: Fast and Generalizable
One-Shot Image to 3D Object Structure via HyperNetworks

Anonymous CVPR submission

Paper ID 1001

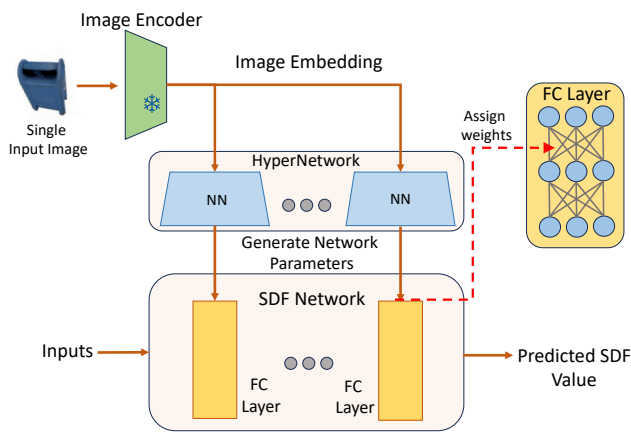


Figure 1. The detail of our HyperNetwork architecture to assign weights to the SDF network. The input is obtained from the image embedding of an image encoder.

In the main manuscript, we have provided the pipeline of our work and in this supplementary material, we provide the details of our method, settings, and additional results.

1. Details of Our Proposed Modules

In the main paper, we mentioned two modules constructing our framework to improve both generalization and consistency. We would detail out these two modules namely HyperNetworks and Voltran in the following sections.

1.1. HyperNetworks

The HyperNetworks [?] are used in our pipeline to build the SDF network. In each HyperNetwork module for each SDF network layer, we build 3 fully-connected layers with ReLU activations in the intermediate layers. In the first layer, we map from the output dimension of the text embedding which is 768 to 32 as the dimension of the hidden layer. The input to the HyperNetwork is the image embedding as an output of an image encoder (e.g., CLIP [?]).

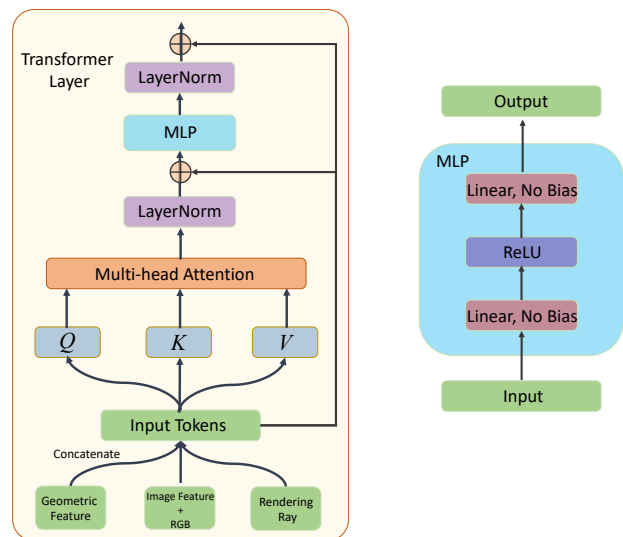


Figure 2. The detail of our Volume Transformer **VolTran** architecture as an aggregator from the features of multiple views.

Please see Fig. 1 for an illustration of our method.

1.2. VolTran: Multi-View Transformer

The transformer module in our framework is used as an aggregator to reduce the noise impacts in multi-view synthesized images. The transformer module is fed with input tokens from the feature of each view. Fig. 2 shows the detail of each component in the transformer module in VolTran. We set the multi-head number to 5 and 2 layers of the transformer with self-attention.

2. Ablation on the Loss Terms

We investigate the role of each loss function to produce high-quality images. We observe that without sparseness regularization term as described in the main paper impacting the capability in generating compact surfaces. As shown in Fig. 5, some object surfaces have some defects and im-

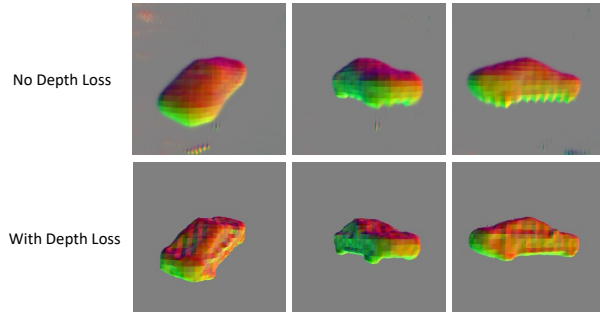


Figure 3. Comparison of including the depth loss and without the depth loss in the training stage. Without the depth loss, the shape becomes more rough and less detailed. The generated 3D scene has some residuals outside the boundaries of the shape.

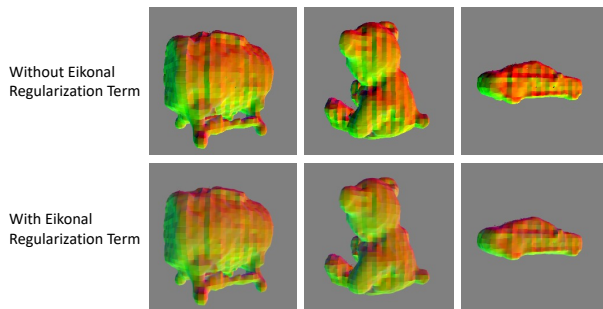


Figure 4. Comparison of including the Eikonal regularization term for smoothness in the training stage. We can observe that the upper part has very rough surface (see the high contrast between dark and bright regions of the surface) and less smooth compared to the below one trained using the Eikonal regularization term.

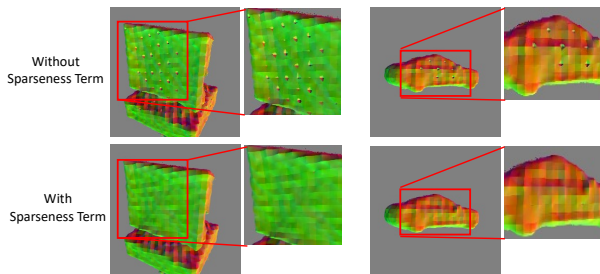


Figure 5. Comparison of including the sparseness regularization term for compactness in the training stage. We observe that the generated surface has some defects (*i.e.*, holes) compared to the below one trained using the sparseness regularization term.

033 pact compactness of the surface because of the uncontrol-
 034 lable free surfaces when we remove the sparseness regular-
 035 ization term. For the Eikonal term, it is applied to regularize
 036 the SDFs and the network to have the unit l_2 norm gradient
 037 yielding smooth surfaces. We experimented to train the net-
 038 work without the Eikonal term, as a result, Fig. 4 shows
 039 that the objects have very rough surfaces due to unregular-

ized SDFs. We also observe that the shape details of an
 040 object might not be accurately predicted without the depth
 041 loss. We also notice that the depth loss enriches the shape
 042 of an object to add more details and remove some unwanted
 043 residuals as shown in Fig. 3. 044

3. Implementation and Evaluation Details 045

3.1. Hyperparameters 046

In our experiments, we use 32 images as the optimal number
 047 of generated images from the outputs of a generative model.
 048 For training the model, we set the learning rate to $5e-4$ and
 049 adjust it using the Cosine learning schedule. The model
 050 is trained for 300K iterations. We set the sparseness term,
 051 Eikonal term, and depth term to 0.02, 0.1, 1.0, respectively.
 052 The background ratio is set to 0.3. 053

3.2. Data Used for Evaluation 054

We opt to use two datasets for our evaluation. The first
 055 dataset is obtained from 15 images proposed in RealFu-
 056 sion [?], intended for evaluating rendering quality. For the
 057 GSO dataset [?], we pick 25 images from different cate-
 058 gories as follows: Alarm, Backpack, Bell, Blocks, Chicken,
 059 Cream, Elephant, Grandfather, Grandmother, Leather, Lion,
 060 Lunchbag, Mario, Oil, Schoolbus1, schoolbus2, Shoeblack,
 061 Soap, Sofa, Sortingboard, Stacking cups, Teapot, Toaster,
 062 Train, Turtle. 063

4. Additional Results 064

In this section, we provide some more detailed images and
 065 more results in addition to the results provided in the main
 066 paper. We provide a zoomed version of the generated results
 067 in comparison to baselines in Fig. 6. We also show all of
 068 our generated results on text-to-3d and image-to-3d tasks in
 069 Fig. 7 Note that we also generate our results and comparison
 070 in the videos. Please see our generated video format. 071



Figure 6. Comparison of our proposed method **Hyper-VolTran** against baselines with zoomed patches.

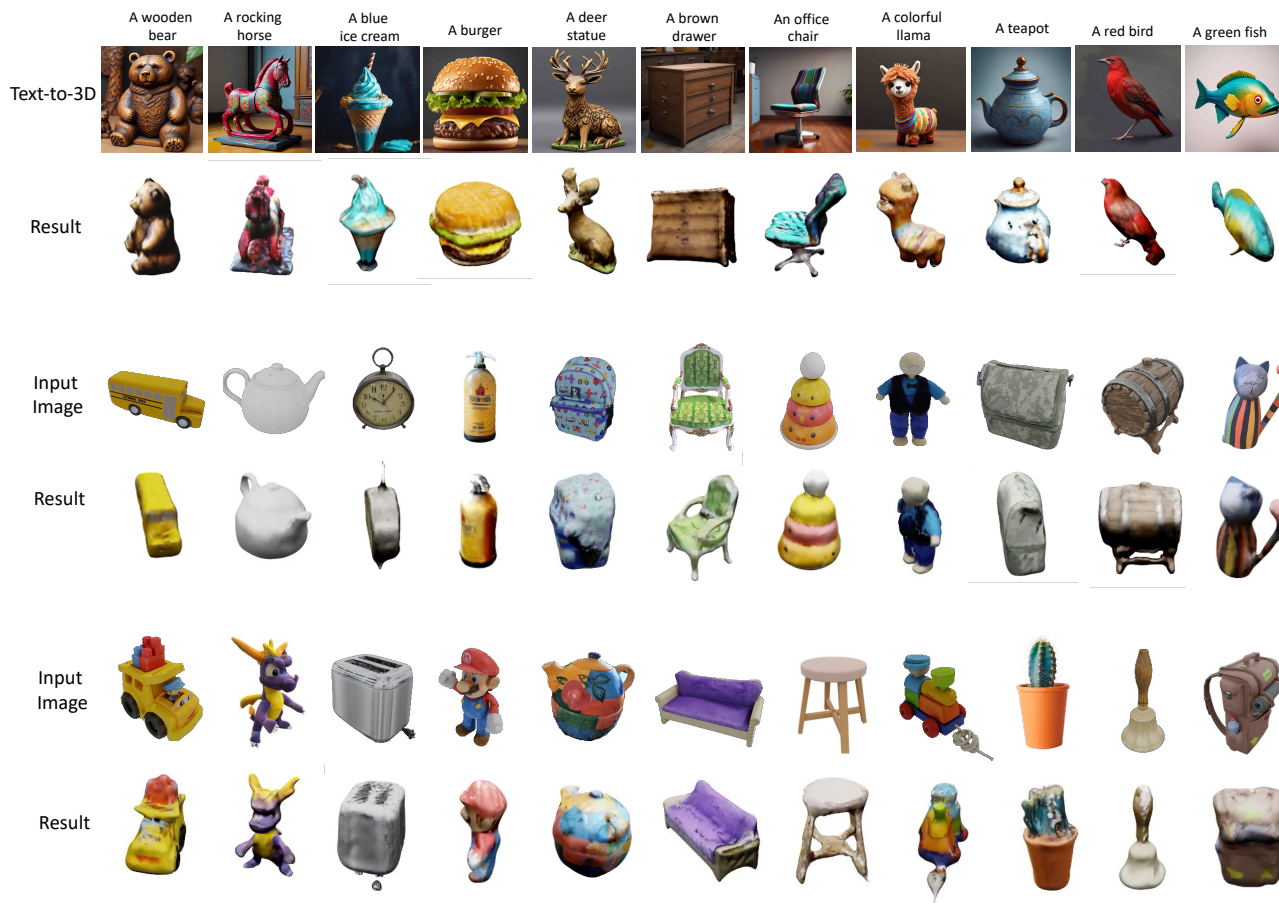


Figure 7. The results of generated 3D objects using our proposed method on text-to-3d and image-to-3d tasks.